NJC

Accepted Manuscript

This article can be cited before page numbers have been issued, to do this please use: Y. Sikdar, R. Goswami, R. Modak, M. Basak, M. J. Heras Ojea, M. Murrie and S. Goswami, *New J. Chem.*, 2018, DOI: 10.1039/C8NJ02955E.

ROYAL SOCIETY OF CHEMISTRY

rsc.li/njc

DOI: 10.1039/C8NJ02955E

NJC

ARTICLE

Diazine based ligand supported Co^{II}_3 and Co^{II}_4 coordination complexes: role of the anions†

Received 00th January 20xx,
Accepted 00th January 20xx

DOI: 10.1039/x0xx00000x

www.rsc.org/

Yeasin Sikdar,[a] Ranadip Goswami,[a] Ritwik Modak,[a] Megha Basak,[a] María José Heras Ojea,[b] Mark Murrie,*[b] Sanchita Goswami*[a]

We report the synthesis and characterisation of a family of three Co^{II}_4, two Co^{II}_3 complexes from an symmetrical diazine ligand, H_2hyda = N,N−bis(3−methoxy salicylidene) hydrazine). The metallic skeletons of all complexes describe a nearly linear arrangement of Co^{II} centers. The present results highlight the profound influence of the anions on the structural outcome of a complex. Furthermore, the distortion imposed by the twisted nature of the diazine based ligand depends on the use of associated anions which results in triple helical Co^{II}_4 and double helical Co^{II}_3 entities. The Co^{II} ions in complexes **1**–**3** are antiferromagnetically coupled leading to diamagnetic ground state. In contrast, complexes **4** and **5** exhibit a magnetic ground state, but exhibit different behaviour at low temperatures due to differences in crystal packing and hence intermolecular interactions.

Introduction

There is continued interest in understanding the rational design of coordination compounds with desired, well defined magnetic properties like single−molecule magnetism,[1] single−ion magnetism,[2] molecular cooling,[3] quantum computing,[4] magnetocaloric effect,[5] spin crossover,[6] etc. In this context, Co^{II} coordination complexes continue to reveal new possibilities because of the potential magnetic anisotropy of Co^{II} ions and this anisotropy can be tuned by spin−orbit coupling to contribute to the overall magnetic behavior.[7] Efforts have been focused on developing Co^{II} complexes with specific arrangement of the anisotropy vectors that are believed to play an important role in determining their magnetic properties and in this regard, structurally simple molecules are currently of interest.[8] Literature reports of coordination compounds of Co^{II} present a rich family to study the influence of chemical modification on the magnetic properties, which illustrates the potential of Co^{II} center(s). Several examples featuring Co^{II} SMMs/SIMs demonstrated large and tunable anisotropy of Co^{II} afforded by deliberate modification of coordination geometry, degree of structural distortion and ligand field strength.[9]

To obtain desired magnetic materials, many efforts have been devoted to design appropriate bridging ligands that play an essential role in dominating the exchange interactions. In this context, halides,[9w] nitrates[10] and carboxylates[11] are long been appreciated for constructing polynuclear complexes that hold inherent structural beauty and ideal model systems for the studies of magnetism. With such considerations in mind, in this work, we evaluated the scope of anion variation on the structural features of three Co^{II}_4 and two Co^{II}_3 coordination compounds. We have employed a diazine based ligand, N,N−bis(3−methoxy salicylidene) hydrazine (H_2hydva), that could enforce helical structure[12] and strategically chosen anions, NO_3^-/Cl^-/Br^- and acetate/pivalate to assess the role of anions.

Results and discussion

Ligand design aspects

Schiff base ligands incorporating the *o*−vanillin moiety has enriched coordination chemistry by providing discrete molecules to coordination polymers in both homo and heteronuclear assemblies.[13] Recently, we have explored the use of *o*−vanillin with both aliphatic and aromatic alcohol amines (2−amino ethanol, 3−amino propanol, 2−amino benzyl alcohol) to synthesise Cu_6Dy_3, Cu_4Dy,[14a] Co_4, Co_7 and $Co^{II}_2Ln^{III}$ complexes (Ln^{III} = Nd^{III}, Sm^{III}, Gd^{III}, Tb^{III}, Dy^{III}).[14b] In light of these results, we were prompted to undertake a new perspective to investigate what happens when *o*−vanillin is dimerised by means of hydrazine to form a diazine ligand.

[a] Department of Chemistry, University of Calcutta, 92, A.P.C. Road, Kolkata, India. E-mail: sgchem@caluniv.ac.in
[b] WestCHEM, School of Chemistry, University of Glasgow, University Avenue, Glasgow, UK . E-mail: mark.murrie@glasgow.ac.uk

†Electronic Supplementary Information (ESI) available: [FTIR, PXRD, ESI-Ms, BVS calculation, protonation level, Shape calculation and crystallographic parameter of complex **1**-**5**; Molecular structure and selected metric parameters of complex **2**,**3**,**5**; Supramolecular figures of **1**-**3**,**5**, magnetization plot of **1-5**; AC magnetic susceptibility plot of **4** and **5**]. CCDC for 1826188-1826190(**1**-**3**), 1826192-1826193(**4**-**5**). For ESI and crystallographic data in CIF or other electronic format see DOI: 10.1039/x0xx00000x

View Article Online
DOI: 10.1039/C8NJ02955E

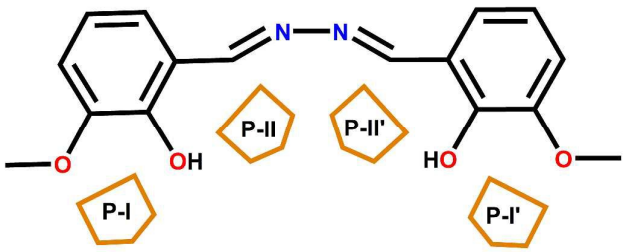

Scheme 1: Coordination pocket of ligand H_2hydva used in this work.

A literature survey on similar diazine ligands based on salicylaldehyde always produced dinuclear helicates.[12] Our goal in this paper was to explore the chemistry of N,N–bis(3–methoxy salicylidene) hydrazine (H_2hydva) towards Co^{II} in presence of two different sets of anions.

H_2hydva contains six coordination sites, namely two N_{imine}, two $O_{phenoxo}$ and two $O_{methoxy}$ to act as multipocket symmetrical ligand system having two distinct coordination environments (see Scheme 1). This makes it a ditopic ligand for binding to hard Mn^{3+}, Co^{3+} and lanthanides ions (see P–I/I' in Scheme 1), and soft +2 oxidation state 3d metal ions (see P–II/II' in Scheme 1). H_2hydva primarily acts as a chelating ligand to bind the metal centers in a helical manner by adopting a twisted conformation when viewed along the N–N bond vector. Several research groups have utilised this ligand to synthesise both homometallic and heterometallic coordination complexes which include Dy_4,[15a] $Dy_{10}Co_2$,[15b] RE_2M_2 (RE = Gd, Tb, Dy, Y; M = Co, Ni, Cu, Zn)[15c] and Cu_3.[15d] (See Scheme S1 in the ESI) But as far our knowledge goes, these complexes are the first Co^{II} only structures derived from this ligand. Additionally, it should be highlighted here that despite a good number of tetranuclear Co^{II}_4 complexes offering open/closed cubane structures are reported in the literature,[7e,9b,9s,9t,14b] open, linear type of Co^{II}_4 systems are scanty.[9w,15e] Here the twisted conformation of the diazine ligand induced the Co^{II} centers to adopt linear arrangement.

Synthetic aspects and characterisation

The reaction of H_2hydva with different Co^{II} precursor salts in alkaline methanol/dichloromethane medium at room temperature yields tetra (**1**–**3**) and tri (**4**–**5**) nuclear Co^{II} complexes as described by equations 1, 2, 3. Our approach was to employ two different kinds of anions (NO_3^-/Cl^-/Br^- and CH_3COO^-/$(CH_3)_3CCOO^-$) to investigate their roles in directing the structure of the complex as well as in magnetic properties. Interestingly, Co^{II}_4 species are generated from NO_3^-/Cl^-/Br^- (**1**, **2** and **3**) whereas the use of carboxylates (CH_3COO^-/$(CH_3)_3CCOO^-$) leads to the formation of Co^{II}_3 complexes (**4** and **5**). Structural diversity is hence created through substrate selection. Usually the pivalate ligands offer structural rearrangement in polynuclear chemistry over its lighter analogues like acetates,[16a] but this strategy does not hold in case of **4** (acetate complex) and **5** (pivalate complex).

While optimizing the reaction conditions for the formation of **1**–**5**, it was noticed that although the formation of the complexes is independent of the metal (M) to ligand (L) ratio, the ratio M : L : Et_3N = 3 : 2 : 4 leads to maximum yield and pure products. It is worth mentioning that the synthetic method adopted for **1**–**3** also generated **4** and **5** but the single crystals were too small to mount. However, the reverse addition process yielded good quality crystals of **4** and **5**. **1**–**5** are air stable and electrically non–conducting in solutions.

$$3H_2hydva + 4CoX_2 + 6Et_3N + 2MeOH = [Co_4(hydva)_3(X)_2(MeOH)_2] + 6[(Et_3NH^+)(X^-)] \quad (X = NO_3, Cl, Br) \quad \cdots\cdots (1)$$

$$2H_2hydva + 3Co(AcO)_2 + 4Et_3N + 2MeOH = [Co_3(hydva)_2(AcO)_2(MeOH)_2] + 4[(Et_3NH^+)(AcO^-)] \quad \cdots\cdots (2)$$

$$4H_2hydva + 3[Co_2(H_2O)(OOCCMe_3)_4(HOOCCMe_3)_4] + 20Et_3N + 4MeOH + H_2O = 2[Co_3(hydva)_2(OOCCMe_3)_2(MeOH)_2] + 2H_2O + 20[(Et_3NH^+)(Me_3CCO_2^-)] \cdots (3)$$

To the best of our knowledge, **1**–**3** are first reported coordination complexes of this new topology and highest nuclearity reported for homometallic compounds of diazine based ligands. (*vide infra*)

FTIR spectra of H_2hydva and **1**–**5** are depicted in Figure S1, in the ESI. The presence of metal bound methanol and lattice water molecule (for **5** only) in the 3420–3440 cm^{-1} region for complexes **1**–**5**, is attributed to $\bar{\nu}_{O-H}$ stretching frequency (*vide infra*). The characteristic peak of H_2hydva at 1623 cm^{-1} assignable to C=N stretching frequency gets decreased to lower wavenumber region of 1586–1610 cm^{-1} in **1**–**5** signifying metal coordination. Complexation through phenolic C–O was supported by the red shift of the ligand peak centered at 1255 cm^{-1} to 1247–1238 cm^{-1} region in **1**–**5**. **1** exhibits a peak at 1384 cm^{-1} attributable to metal bound covalent nitrate. The symmetric $\bar{\nu}_{s(COO)}$ and asymmetric $\bar{\nu}_{as(COO)}$ stretching modes for 1,3 acetate for **4** were detected at 1440 and 1575 cm^{-1} respectively while for the pivalate complex, they were found at 1388 and 1544 cm^{-1} respectively. The difference between smaller asymmetric and symmetric stretching of 135 cm^{-1} and 156 cm^{-1} for **4** and **5** confirms the presence of μ_{1-3} bidentate binding rather than monodentate mode which leads to a greater separation of 350 cm^{-1}.[16b]

In order to verify the phase purity of the synthesised complexes with the calculated single crystal data, powder XRD were performed on powdered sample using Cu–K_α as source. It was observed that, for all the complexes, the peak positions match well with the calculated pattern from SC-XRD data but the noise/scattering was high (Figure S2–S3 in the ESI).

Solid state structural descriptions

Crystallographic data for **1**–**5** are tabulated in Table S1 in the ESI. It will be convenient to discuss the crystal structures of **1**–**3** and **4**–**5** in comparison to determine the structural change in lieu of anion variation. We will elaborate the structures of **1** and **4** in detail while mentioning the notable differences within **1**–**3** and **4**–**5**.

View Article Online
DOI: 10.1039/C8NJ02955E
NJC ARTICLE

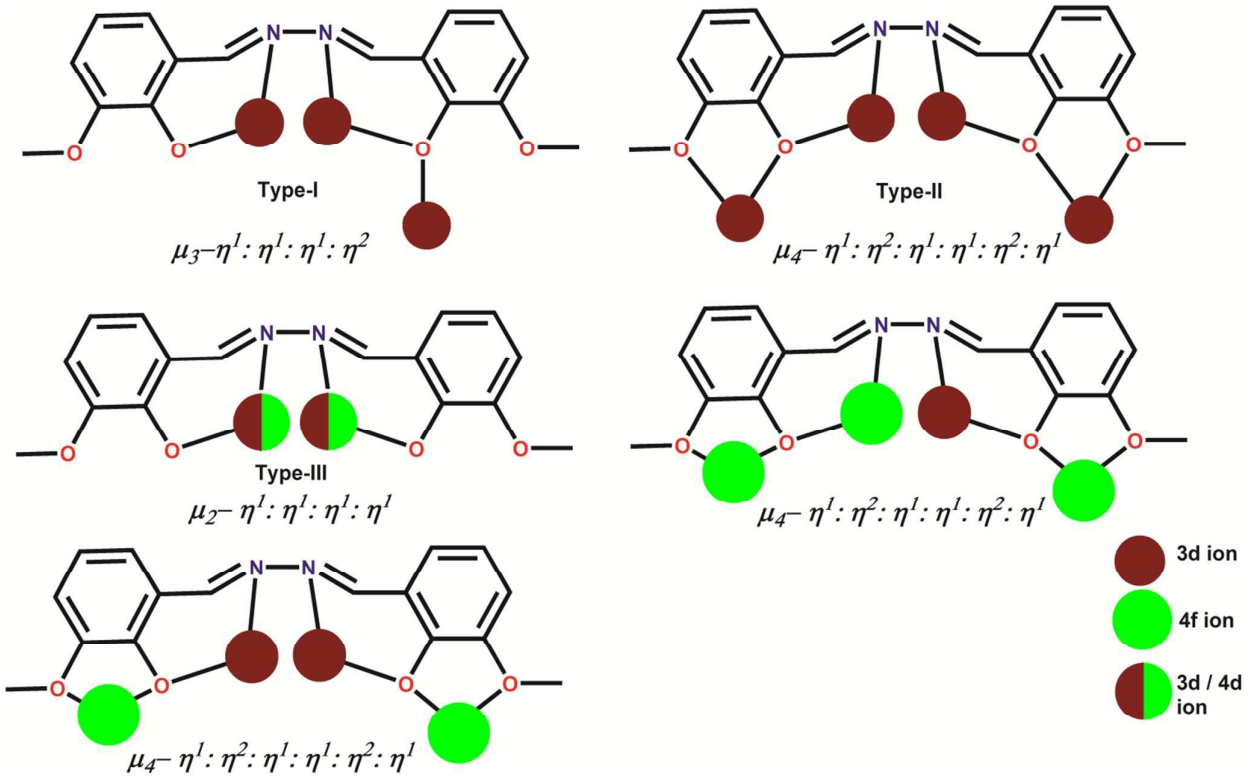

Scheme 2: Binding mode of the deprotonated form of the ligand H_2hydva encountered in this work (Type–I–II) and in the literature.

The solid state molecular structure of **1** reveals an open, linear type, tetranuclear Co^{II}_4 motif encapsulated by three hydva^{2-} ligands (see Figure 1, Table S12 and S13 in the ESI). Here, hydva^{2-} ligands utilise two different coordination modes, μ_3–η^1: η^1: η^1: η^2 (Type–I) and μ_4–η^1: η^2: η^1: η^1: η^2: η^1 (Type–II), to bind four Co^{II} centers (see Scheme 2). As depicted in Scheme 2, one hydva^{2-} spans the entire Co^{II}_4 whereas the remaining two ligands partially support the core. The coordination environment of the four Co^{II} ions can be classified as: (a) the terminal Co^{II} centers (Co1 and Co4) are surrounded by $O_{phenoxo}$ (O6/O11), N_{imine} (N3/N6) of one ligand, μ–$O_{phenoxo}$ (O2/O3) and $O_{methoxy}$ (O1/O4) of other ligand along with an asymmetrically capped nitrate ion (Co1–O15 2.230(3) Å, Co1–O16 2.284(4) Å, Co4–O18 2.138(9) Å, Co4–O19 2.351(7) Å) (see Table S2 in the ESI).[17] Continuous Shape Measurements (CShMs) were performed to predict the geometry around the Co^{II} centres (see Table S7 in the ESI) which indicated distorted trigonal prismatic geometry (D_{3h}) around the hexacoordinated Co1 and Co4. The basal square plane is constituted by O6O1O2N3 for Co1 and O3O4O11N6 for Co4 and they are lifted from their least square planes by 0.5228(4) Å and 0.5526(5) Å respectively. (b) The closest geometry of the inner cobalt centers (Co2/Co3) could be assigned as distorted octahedron coordinated by $O_{phenoxo}$ (O2,O7/O3,O10) and N_{imine} (N4,N1/N5,N2) of two ligands, $O_{phenoxo}$ (O10/O7) of another ligand and a coordinated methanol (O13/O14) molecule, as dictated by the smallest CShMs value of 0.981/0.913 (see Table S7 in the ESI). The Co–O/N bond distances are typical for Co^{II} centers and compare favourably with the bond parameters found in other Co^{II} coordination complexes[11] while Co···Co bond distances ranging from 2.996–3.398 Å.

The hydva^{2-} ligands adopt a twisted conformation when viewed along the N–N bond vector and the extent of the helical twist of the three ligands chelating four cobalt centers is different. The torsional angles of the diazine moieties in the terminal ligand have the values of 58.4(3)° (chelating Co1 and Co2) and 58.6(3)° (Co3 and Co4). However, the ligand chelating inner Co2 and Co3, has a dihedral angle of 55.3(3)° around the N–N bond. This difference in the dihedral angles, restricts the D_3 symmetry expected for a perfect triple helicate[12a] (see Figure 1). Thus, the formation of the Co^{II}_4 complex can be described as the dimerisation of two puckered Co^{II}_2 units through double phenoxo and diazine bridges. Two puckered pentagonal Co^{II}_2 units are connected by a μ–phenoxo bridge with a dihedral angle of 45.99° and further chelated by a hydva^{2-} ligand to form a $Co_2N_2O_2$ core. The dihedral angle between the two terminal planes passing through the dimeric unit is 13.60(8)°.

View Article Online
DOI: 10.1039/C8NJ02955E

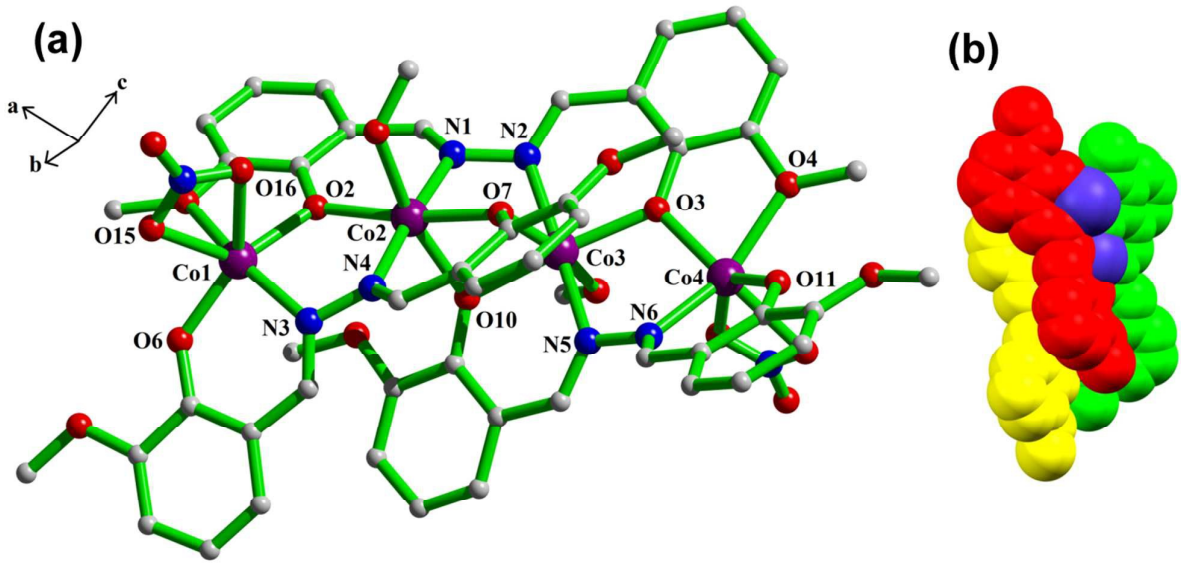

Figure 1: (a) Molecular structure of complex **1** in ball and stick model. Hydrogen atoms associated with carbon atoms have been removed for the clarity. (b) Complex **1** in a space fill model, where each of the ligands are shown in different colours to emphasize the triple helicate coordination structures, methanol and nitrate ligands are not shown for the sake of clarity.

In **2/3**, Cl^-/Br^- ligands are present in place of NO_3^-. While the basic metallic skeletons are similar, there is nonetheless a distinct difference between **1** and **2/3**. Here, the outer Co^{II} centers (Co1 and Co4) bears five coordinated environment composed of two $O_{phenoxo}$ (one μ–bridged and another singly μ_1), one N_{imine} and $O_{methoxy}$ group of diazine ligand and halide ion (Cl^- for **2**, Br^- for **3**) (see Figure S4 and S5 in the ESI). From the CShMs analysis, Co1 and Co4 correspond best to square pyramidal (C_{4v}) geometry (see Table S8–S8 in the ESI).

The crystal structure of **4** was determined in the centrosymmetric triclinic *P*–1 space group with two crystallographically independent Co^{II} centers (Co1 and Co2) in the lattice while **5** crystallises in the orthorhombic *Pca2₁* space group where each of the cobalt centers (Co1, Co2 and Co3) is crystallographically independent (see Figure 2 and Figure S6 in the ESI). In **4**, the doubly deprotonated ligand utilises only the type–I bridging mode to form the trinuclear array. The asymmetric unit of **4** consists of one doubly deprotonated ligand $hydva^{2-}$, one μ_2–bridging acetate, one coordinated methanol, one occupied Co1 and one Co2 with half occupancy. The peripheral cobalt centers (Co1 and Co1$^{\#}$) adopt a highly distorted octahedral geometry with an NO_5 coordination set provided by μ–$O_{phenoxo}$ and N_{imine} of one ligand, μ–$O_{phenoxo}$ and $O_{methoxy}$ of the other ligand, while the fifth and sixth coordination sites are supported by one methanol and bridging acetate respectively. The central Co2 resides in compressed octahedral environment with three *trans* angles of 180° while the *cis* angles vary from 87.22(13)° to 92.78(13)°.

The octahedral geometry is constituted by two N_{imine} atoms, two μ–$O_{phenoxo}$ of two $hydva^{2-}$ ligands and two bridging acetates. The bridging acetate caps the inner and outer cobalt atoms in μ_2–*syn*–*syn*–η^1:η^1 fashion with bond distances 2.119(3) and 2.073(3) Å respectively.

CShMs calculations were employed to infer the coordination geometry around the metal centers. The central Co2 has the smallest CShMs value of 0.249 suggesting a distorted octahedron (O_h). The coordination polyhedron around the terminal Co1/Co1$^{\#}$ centers is close to an distorted octahedron (O_h) (CShMs value 4.177/4.176). The presence of one significantly longer Co–$O_{methoxy}$ bond distance of Co1–O4 2.415(4) Å prompted us to search in the CSD for Co–O distances in complexes displaying hexacoordinate Co(II) centres with phenoxo/vanillin ligands. The CSD results display that one of the most common Co–OMe distance is around 2.41 Å, reaffirming our distorted octahedral assignment (see Table S10 in the ESI).

Here also the ligand $hydva^{2-}$ adopts a twisted conformation to bind the central and peripheral cobalt centers where the torsion angle is 50.4(6)°. This twisting reinforces the displacement of outer cobalt atom (Co1) by 0.7794(6) Å from the least square plane of Co2 constituted by N2O3N2$^{\#}$O3$^{\#}$Co2. The metallic core reveals the presence of two puckered pentagonal $Co_2N_2O_{phenoxo}$ units of dihedral angle of 35.31(9)° (angle between mean Co1O3Co2 and Co1N1N2Co2). These units dimerise via the central Co^{II}, bearing C_2–axis in a twisted manner resulting in a perfectly linear Co^{II}–Co^{II}–Co^{II} arrangement (180°) with Co···Co distance of 3.345 Å that finally gives rise to double helical structure (see Figure 2).

Complex **5** features pivalate instead of acetate (see Figure S6 in the ESI). As described in **4**, all the Co^{II} ions are in a hexacoordinated environment. Note that, although the Co–OMe distances in **5** (Co1–O8 2.489(5) Å, Co3–O4 2.480(5) Å) are slightly longer than those observed in **4**, the pentacoordinated geometry around the outer Co1, Co3 ions is discarded since the difference is not significant (~0.06 Å). Also, the Co–OMe distances in **5** are still reasonable considering similar reported structures. Therefore, as per CShM analysis, all the Co^{II} ions display an octahedral arrangement of ligands (seeTable S11 in the ESI).

View Article Online
DOI: 10.1039/C8NJ02955E
NJC ARTICLE

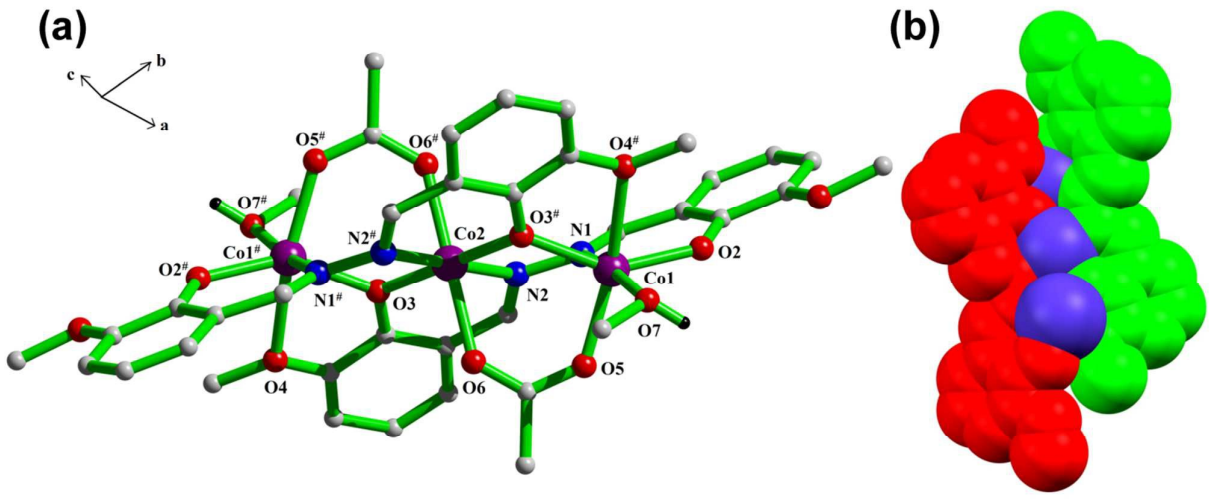

Figure. 2: (a) Molecular structure of complex **4** in a ball and stick model. Hydrogen atoms associated with carbon atomshave been removed for the clarity. (b) Complex **4** in a space fill model, where each of the ligands are shown in different colours to emphasize the double helicate coordination structures, coordinated methanol and acetate molecule is not shown for the sake of clarity. Symmetry operator for equivalent position, #: (1−x, 1−y, 1−z).

Supramolecular Description

The crystal packing of **1**, **2** and **3** was further stabilised by strong inter−molecular C−H···π interactions between the $-CH_3$ of –OMe group and the adjacent phenyl ring. This gives rise to 1−D supramolecular chains in a zig−zag fashion along crystallographic axis *a* and they are involved in inter chain interactions through aromatic C−H····π to form a corrugated sheet like structure (see Figure S7, Figure S8, Figure S9 in the ESI). In **4** the adjacent molecules form 1−D supramolecular chains through hydrogen bonding between the oxygen atom of acetate and the hydrogen atom of coordinated methanol molecule and these 1−D chains undergo C−H···O interaction along *b* axis to form 2−D sheet over *bc* plane (see Figure 3). The crystal lattice of **5** is stabilised by the strong hydrogen bonding between the lattice water (both donor and acceptor) and acetate (acceptor)/methanol (donor) of the molecule to form a zigzag chain along *c* axis. C−H···O interaction between the 1−D chains gives rise to 2−D sheet along *ac* plane (see Figure S10 in the ESI).

Mass−spectrometric analysis

Mass spectrometry studies were performed to determine the principal species present in solution and investigate the fragments which combined during the synthesis and crystallisation process. Mass spectra for **1**−**5** are recorded in methanol (see Figure S11−S15 in the ESI). Complexes **1**−**3** offered identical peaks at 1072.13 amu (calcd. 1072.09) and 1094.11 amu (calcd. 1094.08) which can be identified as $[Co_3(hydva)_2(Hhydva)]^+$ and $[Co_3(hydva)_3+Na]^+$ respectively. The $[Co_3(hydva)_2(Hhydva)]^+$ species appears as base peak in **1** while for **2** and **3** its relative intensities are 50% and 40% respectively. The $[Co_4(hydva)_3]^{2+/1+}$ fragment is not detected in the ESI−MS spectrum probably due to the instability of the gaseous ion on the ESI−MS timescale. The base peak for **4** appeared at 818.02 amu (calcd. 817.99) assignable to $[Co_3(hydva)_2(OAc)-Me]^+$ where an –OMe group of one *o*−vanillin moiety gets hydrolysed. Similarly two –OMe hydrolysed fragmented peaks also appeared at 804.03 amu and identified as $[Co_3(hydva)_2(OAc)-2Me]$ fragment. We are unable to detect the molecular ion peak of **4**. For **5**, the peak at 998.17 amu (calcd. 998.07) is attributed to the species $[Co_3(hydva)_2(Piv)_2+Na]^+$ which appears as molecular ion peak while the base peak appears at 874.13 amu (calcd. 874.05), which is assigned to $[Co_3(hydva)_2(OOCCMe_3)]^+$. In both **4** and **5**, a dipositive peak of $[Co_3(hydva)_2]^{2+}$ in small intensity appeared at 386.49 amu (calcd. 386.49). In all the species mentioned above, the expected isotopic pattern matches excellently with

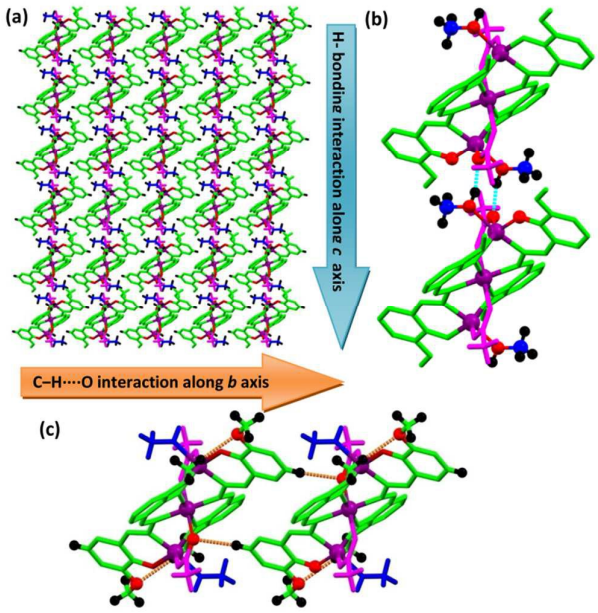

Figure. 3: (a) 2-D supramolecular architecture formed by complex **4** in the *ac* plane. (b) The zig-zag nature of the 1-D chain propagated along crystallographic axis a connected through C-H-π interactions. (c) The zoom view of each of the 1-D chain stabilized by inter molecular C−H···π interaction between the $-CH_3$ of –OMe group and the adjacent phenyl ring along the crystallographic axis *c*.

View Article Online
DOI: 10.1039/C8NJ02955E

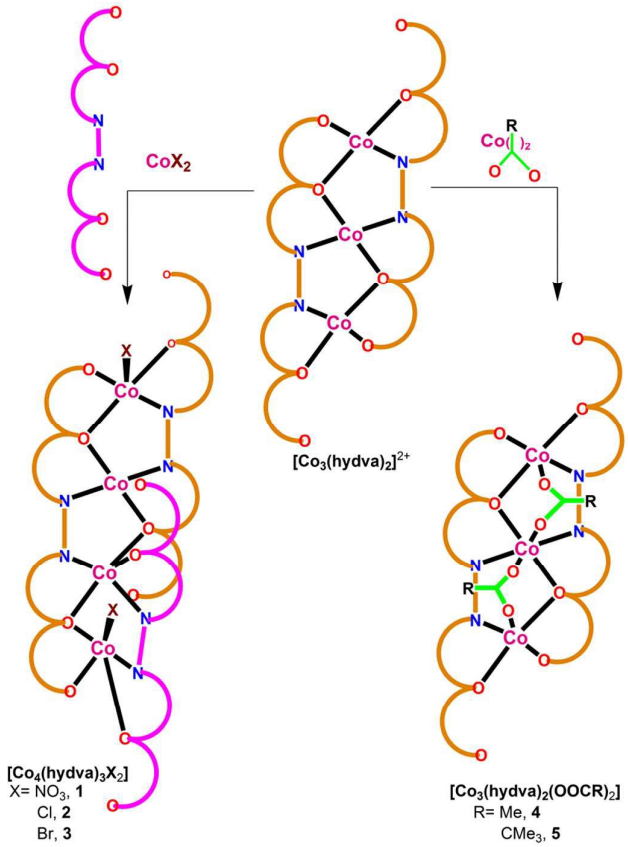

Scheme 3: Possible mechanism for the formation of the tetranuclear complex from an intermediate trinuclear entity as detected in ESI-MS.

the experimental one indicating the correct assignment of the species.

Anion influence in complex formation and their structural correlation

Finally, we tried to evaluate the structural differences generated on changing the anion from $NO_3^-/Cl^-/Br^-$ to $CH_3COO^-/(CH_3)_3CCOO^-$ (see Table 1). As discussed in the previous section we were able to detect the trinuclear species $[Co_3(hydva)_2(Hhydva)]^+$ or $[Co_3(hydva)_3+Na]^+$ in the mass spectrum. This species plays a key role in the formation of the complexes. When carboxylate ($CH_3COO^-/(CH_3)_3CCOO^-$) combines with this trinuclear species through a 1,3 bridging mode (*via* 6- member ring formation), both the charge and coordination around the metal centre is satisfied. Bridging by means of $NO_3^-/Cl^-/Br^-$ set is characterized by three membered ring formation as well as small bite angle for NO_3^-. Thus, if we compare the bridging abilities between ($NO_3^-/Cl^-/Br^-$) and $CH_3COO^-/(CH_3)_3CCOO^-$ sets, it would be justified to presume that the $CH_3COO^-/(CH_3)_3CCOO^-$ set scores better as bridging entities. Therefore, in case of $NO_3^-/Cl^-/Br^-$ analogues, one more $hydva^{2-}$ and Co^{II} centre combine with the trinuclear fragment to satisfy the coordination and halide or nitrate acts as termination group. This proposal of formation of tetranuclear and trinuclear structures is depicted in Scheme 3.

Table 1: Some comparable parameters of complex **1**–**5**

Atom–Atom	Twist angle of ligand[a] (º)	Bond distance (Å)	$\angle Co-O-Co$ (º)
	Complex 1		
Co1–Co2	58.4(3)	3.398	113.50(8)
Co2–Co3	55.3(3)	2.996	92.46(7)
			91.43(7)
Co3–Co4	58.57(6)	3.366	112.69(9)
	Complex 2		
Co1–Co2	58.4(4)	3.336	111.7(1)
Co2–Co3	56.2(4)	2.984	91.56(8)
			92.77(8)
Co3–Co4	58.3(4)	3.358	112.13(9)
	Complex 3		
Co1–Co2	58.8(6)	3.320	111.8(2)
Co2–Co3	56.6(5)	2.969	91.5(1)
			92.7(1)
Co3–Co4	59.3(5)	3.351	112.4(1)
	Complex4		
Co1–Co2	50.4(6)	3.345	111.60(15)
Co2–Co1[#]	50.4(6)	3.345	111.60(15)
	Complex 5		
Co1–Co2	51.0(8)	3.297	110.3(2)
Co2–Co3	52.6(8)	3.308	110.8(2)

[a]ligand chelating the former atom entry, [#] (1–x, 1–y, 1–z)

As can be seen with increase of twist angle of the ligand, the chelated Co···Co distance and consequently Co–O–Co angle increases for all the five complexes (see previous section). For complexes **4** and **5** *syn–syn* μ_2–1,3–carboxylate bridge and a single phenoxide bridge constitutes the linear arrangement of Co^{II}_3 compounds. The change in carboxylate moiety induces the non planarity in the Co2O1N2 core and deviation of the terminal metal ion from the basal plane of the central metal ion.[18] Thus the terminal Co is 0.7789(6) Å deviated in complex **4** while in complex **5** Co1 and Co3 is deviated 0.8842(6) and 0.8182(6) Å from the least square plane of the central atom respectively. Carboxylate variation has very little impact on change in Co–O–Co angle (for **4**, angle Co–O–Co 111.60(5)°; for **5**, angle Co–O–Co 110.4(2)° and 110.8(2)°). In this context, the presence of a single phenoxo– and acetato–bridged trinuclear Co^{II}_3 arrangement is scarce in the literature. Si *et al*. reported a couple of Co^{II}_3 coordination polymers where the Co–O–Co angle is 117.82(8)° and the adjacent Co···Co distances are 3.853 Å.[17]

Comparison with other diazine based Co^{II} complexes in literature

Complexes **1**–**5** join a small family of compounds containing a diazine based ligand system. Literature reports of diazine based ligands derived from salicyaldehyde show dinuclear coordination complexes of Fe^{III}_2, Mn^{III}_2, Co^{III}_2 *etc.* Utilizing symmetrically two N_{imine} and O_{phen} sites Lin *et al.* reported a Dy^{III}_4 defect dicubane where the central Dy^{III}_4 core is sandwiched symmetrically by two diazine ligands and $O_{methoxy}$ remains uncoordinated. Comparing this with the above mentioned examples, it can be viewed as two Dy^{III}_2 units connected by other auxiliary ligands.[15a] A $Dy^{III}_{10}Co^{II}_2$ complex was

View Article Online
DOI: 10.1039/C8NJ02955E
NJC ARTICLE

reported by Zou *et al.* where all six sites bind Dy^{III}/Co^{II} in almost linear arrays which are connected by acetates to generate a wheel like motif.[15b] In 2015, a series of linear $[RE_2M_2]$ (RE = Gd, Tb, Dy, Y; M = Co, Ni, Cu, Zn) complexes supported by two symmetrical hydva^{2-} ligands were reported.[15c] The same ligand was utilised by Wei *et al.* to produce a linear Cu^{II}_3 complex surrounded by two ligands where one $O_{methoxy}$ from each ligand remained uncoordinated.[15d] But homometallic, tri/tetra nuclear complexes of this ligand with systematic variation of auxiliary ligands are absent from the literature. In this paper, we have reported hydva^{2-} supported Co^{II}_4 and Co^{II}_3 structures utilising two sets of anions, $NO_3^-/Cl^-/Br^-$ and $CH_3COO^-/(CH_3)_3CCOO^-$ respectively to assess the contribution of the anions to the structural outcome. For $NO_3^-/Cl^-/Br^-$ series, one hydva^{2-} spans the entire skeleton utilizing μ_4–η^1: η^2: η^1: η^1: η^2: η^1 mode whereas, the other two ligands partially encompasses the Co^{II} centers via μ_3–η^1: η^1: η^1: η^2 mode (See Figure S16 in the ESI). The outcome of $CH_3COO^-/(CH_3)_3CCOO^-$ series (See Figure S17 in the ESI) resembles the above mentioned Cu^{II}_3 example.

Magnetic Study

The variable–temperature magnetic properties of **1**–**5** were investigated in the range of 290–2 K in an applied field of 1000 Oe (see, plots Figure 4). The experimental values of $\chi_M T$ at room temperature are significantly higher than the calculated spin–only value for four isolated Co^{II} ions (S = 3/2, g = 2; 7.50 $cm^3 \cdot mol^{-1} \cdot K$) in case of the tetranuclear complexes **1**–**3**, and three non–interacting Co^{II} ions for the trinuclear compounds **4** and **5** (5.63 $cm^3 \cdot mol^{-1} \cdot K$), suggesting the presence of magnetic anisotropy. The magnetic anisotropy is confirmed by variable–field measurements (at 2, 4, 6 K in the field range of 0–5 T), since none of the samples reach the saturation magnetisation (see Figure S18 in the ESI). As previously mentioned, the symmetry analyses[19–21] on the cobalt centers for **1**–**5** propose different geometries considering the coordination environment around the Co^{II} ions (see CShMs values in Tables S7–S11 in the ESI). For **1** the two outer hexacoordinate–Co^{II} ions are described as distorted trigonal prism (D_{3h}), and the inner ones as octahedral (O_h). On the other hand, two coordination environments can be observed in **2** and **3**: the outer Co^{II} ions (Co1, Co4) are pentacoordinate in a square pyramidal (C_{4v}) environment, whereas the inner ones (Co2, Co3) are hexacoordinate in an octahedral geometry. Regarding the $\{Co^{II}_3\}$ complexes **4** and **5**, all the three Co(II) centers can be described as distorted O_h. Taking into account the different proposed symmetries, and the corresponding *d*–orbital splitting, the magnetic anisotropy may arise from 1st order spin–orbit coupling (SOC) effects related to those atoms displaying ~O_h symmetry, and from zero–field splitting (ZFS) effects from those ions displaying D_{3h} or C_{4v} geometries. As the temperature is lowered, the $\chi_M T$ products for **1**–**3** decrease gradually with temperature reaching minima of 0.41 $cm^3 \cdot mol^{-1} \cdot K$ (**1**), 0.77 $cm^3 \cdot mol^{-1} \cdot K$ (**2**) and 0.73 $cm^3 \cdot mol^{-1} \cdot K$ (**3**) at 2 K (see Figure 4). This decrease is likely due to a combination of SOC and ZFS effects (see above) as well as antiferromagnetic intramolecular interactions, and is

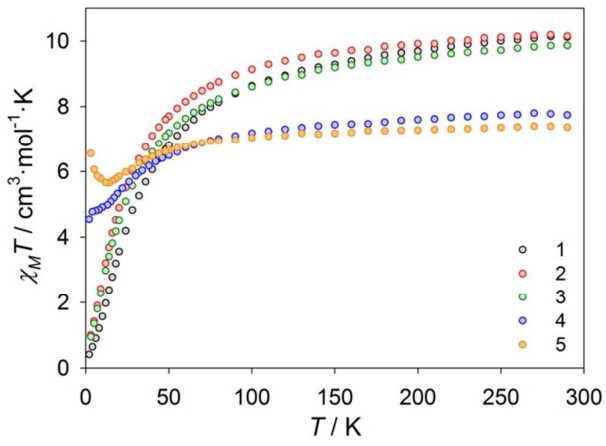

Figure 4. Temperature dependence of $\chi_M T$ for **1**–**5** in an applied field of 1000 Oe.

consistent with a diamagnetic ground state. The experimental $\chi_M T$ values for complex **4** steadily decrease with temperature, before reaching a plateau at ~10 K and a minimum of 4.54 $cm^3 \cdot mol^{-1} \cdot K$ at 2 K. The tendency observed above 10 K is dominated by SOC effects, whereas antiferromagnetic interactions are likely to be responsible for the decrease of the susceptibility values below 10 K. In the case of **5**, a decrease of the $\chi_M T$ values until 13 K is observed (5.65 $cm^3 \cdot mol^{-1} \cdot K$), followed by an increase to reach a maximum of 6.97 $cm^3 \cdot mol^{-1} \cdot K$ at 2 K, consistent with the presence of weak ferromagnetic interactions. Clearly, the $\{Co^{II}_3\}$ complexes (**4** and **5**) exhibit different behaviour at low temperatures. This could arise from differences in the intermolecular interactions due to the different crystal packing displayed by the two complexes. As previously discussed, **4** displays H–bonds between MeOH and AcO^- groups of different molecules, with a Co···Co distance of 5.2261(7) Å. On the other hand, the interaction displaying the shortest Co···Co distance in **5** (6.897(1) Å) is *via* phenoxide and MeOH groups and a water molecule of crystallisation. That leads to an increase of the Co···Co distances, and could lead to different intermolecular interactions.

Considering the non–zero ground state inferred from the $\chi_M T$ values shown by **4** and **5** at low temperatures, the dynamic magnetic properties of both complexes were investigated by ac susceptibility measurements as a function of the temperature (T = 2–10 K) in the absence and presence of an external field (H_{dc}= 2000 Oe) (see Figure S19 and S21 in the ESI). No signal was observed in the out–of–phase susceptibility (χ") for **5** in zero applied dc field (see Figure S21, left in the ESI) or under the influence of an applied field (Figure S21, right in the ESI). In contrast, the application of a field leads to the enhancement of the dynamic properties in **4**, resulting in the appearance of the tail of a frequency–dependent out–of–phase signal (see Figure S19, right in the ESI). Thus, isothermal field sweep *ac* susceptibility experiments as a function of frequency were performed (see Figure S20 in the ESI) towards the suppression of the quantum tunnelling of the magnetisation within the molecule, which may be responsible

View Article Online
DOI: 10.1039/C8NJ02955E

for the null signal in zero applied dc field. Unfortunately, no maximum of the χ" signal was observed despite the application of moderately large field (*i.e.* 5000 Oe) and consequently no further ac studies were performed on **4**.

Conclusions

In this report, we undertook a systematic study of five Co^{II} complexes equipped with a diazine based ligand, N,N–bis(3–methoxy salicylidene) hydrazine (H_2hydva), that has been used to construct helical structures. Reacting H_2hydva with Co^{II} salts of NO_3^-/Cl^-/Br^- gave rise to tetranuclear Co^{II}_4 complexes **1**/**2**/**3**. When we switched to CH_3COO^-/$(CH_3)_3CCOO^-$, we were able to isolate trinuclear Co^{II}_3 compounds. These outcomes underscore the point that the sets of anions NO_3^-/Cl^-/Br^- and CH_3COO^-/$(CH_3)_3CCOO^-$ play distinct structure directing roles in the complexes **1**–**5**. The presence of a twisted diazine type of ligand is the key feature in generating triple helicates in **1**/**2**/**3** and a double helicate structure for **4**/**5**. We have also ventured to analyze the structural differences among **1**/**2**/**3** and **4**/**5** through detailed mass spectrometric studies and justified the structural outcome. Eventually, these are the first Co^{II} based complexes derived from this diazine ligand. The observed structural differences in **1**–**5** lead to different final magnetic properties. The magnetic studies show that the Co(II) ions tends to be antiferromagnetically coupled within the tetranuclear $\{Co_4\}$ family (**1**–**3**), considering the S ~ 0 ground state at 2 K. Complexes **4** and **5** exhibit a different behaviour at low temperatures despite their similar $\{Co^{II}_3\}$ arrangement: intermolecular antiferromagnetic Co···Co interactions seem to be favoured in **4**, whereas weak intermolecular ferromagnetic interactions are in **5**. The different intermolecular interactions at low temperature may be a consequence of the changes in the H–bonds arising from the different crystal packing.

We believe that the outcome of the present work would provide important insight to the synthetic chemists for optimizing the synthetic route. Future work involving related ligands will be focussed on varying other synthetic parameters for a comprehensive understanding of the systems.

Experimental Section

Chemicals and general instrumentation

All starting materials were obtained from commercial sources and were of synthesis grade and used as received without further purification. Solvents were dried following standard procedures. All manipulation was performed under aerobic condition. $[Co_2(H_2O)(OOCCMe_3)_4(HOOCCMe_3)_4]$ was prepared as previously described.[22] The hexadentate ligand (H_2hydva = *N*,*N*–bis(3–methoxy salicylidene) hydrazine) was synthesised according as previously described.[15c] The ligand was further purified by recrystallisation from hot chloroform to give needle–like yellow crystals. Elemental analysis for carbon, hydrogen and nitrogen was carried out on a Perkin–Elmer 2400 II analyzer. FT–IR spectra were recorded on Perkin Elmer Spectrum 100 spectrophotometer on KBr disk. Powder X–ray diffraction (PXRD) patterns were acquired using a PANalytical, X'PERT diffractometer (Netherlands) operated at 40 kV, 30 mA, with graphite–monochromatised Cu–K_α radiation of wavelength = 1.5418 Å and a nickel filter. ESI–MS was performed on a Waters Xevo G2–S QTOF instrument in LC–MS grade solvent.

Synthesis of complexes

$[Co_4(hydva)_3(NO_3)_2(MeOH)_2]$ (1)

H_2hydva (0.15 mmol, 0.049 g) was dissolved in 10 mL dichloromethane. To this yellow solution $Co(NO_3)_2{\cdot}6H_2O$ (0.225 mmol, 0.065 g) in 5 mL of methanol was added and the solution became reddish. Then 0.3 mmol (42µL) of Et_3N was added to it and vigorously stirred for 3 hrs. The volume was reduced on a rotary evaporator at a temperature below 35°C and layered with diethyl ether. Reddish–brown block crystals suitable for single crystal XRD study were obtained after 4 days. Crystals were separated by filtration and quickly washed with copious amount of ice cold methanol and dried in a calcium chloride desiccator. Yield: 53 mg (71% based on Co). M.W.–1318.71 g/mol. Elemental (CHN) (%) analysis for $C_{50}H_{50}Co_4N_8O_{20}$: Calcd: C, 45.54; H, 3.82; N, 8.50; found: C, 45.03; H, 4.07; N, 8.75. FTIR (cm^{-1}): 3401, 2930, 1603, 1436, 1245, 1211, 1082.

$[Co_4(hydva)_3(Cl)_2(MeOH)_2]$ (**2**) and **$[Co_4(hydva)_3(Br)_2(MeOH)_2]$** (**3**) were prepared according to the procedure described for complex **1** using $CoCl_2{\cdot}6H_2O$ and $CoBr_2{\cdot}6H_2O$ respectively instead of $Co(NO_3)_2{\cdot}6H_2O$. The analytical data of the complexes are given below:

$[Co_4(hydva)_3(Cl)_2(MeOH)_2]$ (**2**)

Yield: 47 mg (65% based on Co). M.W.–1265.6 g/mol. Elemental (CHN) (%) analysis for $C_{50}H_{50}Cl_2Co_4N_6O_{14}$: Calcd: C, 47.45; H, 3.98; N, 6.64; found: C, 47.93; H, 3.65; N, 6.98. FTIR (cm^{-1}): 3324, 2927, 1600, 1457, 1437, 1288, 1211, 1082, 739.

$[Co_4(hydva)_3(Br)_2(MeOH)_2]$ (3)

Yield: 43 mg (56% based on Co). M.W.–1354.5 g/mol. Elemental (CHN) (%) analysis for $C_{50}H_{50}Br_2Co_4N_6O_{14}$.Calcd: C, 44.34; H, 3.72; N, 6.20; found: C, 44.07; H, 3.72; N, 6.20. FTIR (cm^{-1}): 3350, 2927, 1603, 1456, 1432, 1243, 1209, 1081, 738.

Complexes **4** and **5** were synthesised with small alterations to the procedure described above.

$[Co_3(hydva)_2(OAc)_2(MeOH)_2]$ (**4**)

H_2hydva (0.15 mmol, 0.049 g) was dissolved in 3 mL of dichloromethane and it was added to a previously prepared 5 mL methanolic solution of $Co(OAc)_2{\cdot}4H_2O$ (56 mg, 0.225 mmol). The colour turns deep red on addition of Et_3N (42µL, 0.3 mmol) and stirring was continued for 3 hrs followed by filtration to remove any insoluble residue. The solution was layered with diethyl ether. After 5 days, X–ray quality deep red crystals were obtained and washed with copious amount of cold methanol and dried under vaccum. Yield: 65 mg (78% based on Co). M.W.–955.55 g/mol. Elemental (CHN) (%) analysis for $C_{38}H_{42}Co_3N_4O_{14}$: Calcd: C, 47.76; H, 4.43; N, 5.86; found: C, 48.23; H, 4.88; N, 5.32. FTIR (cm^{-1}): 3387, 2932, 1578, 1439, 1242, 1208, 1080, 735.

$[Co_3(hydva)_2(OOCCMe_3)_2(MeOH)_2]{\cdot}2H_2O$ (**5**)

View Article Online
DOI: 10.1039/C8NJ02955E

Same procedure as described for **4** was followed using $[Co_2(H_2O)(OOCCMe_3)_4(HOOCCMe_3)_4]$ (107.2 mg, 0.113 mmol) instead of $Co(OAc)_2$. Yield: 50 mg (61% based on Co). M.W.−1075.73 g/mol. Elemental (CHN) (%) analysis for $C_{44}H_{58}Co_3N_4O_{16}$: Calcd: C, 49.13; H, 5.43;N, 5.21; found: C, 48.74; H, 5.01; N, 4.96. FTIR (cm^{-1}): 3418, 2960, 1609, 1542, 1459, 143, 1212, 1109, 736.

Magnetic Measurements

Magnetic measurements for all the complexes (**1–5**) were performed on polycrystalline samples constrained in eicosane, using a Quantum Design SQUID magnetometer equipped with a 5 T magnet. The direct current (dc) measurements were performed in the temperature range 290–2 K under an applied field of 1000 Oe. Field−dependent magnetisation measurements were performed at 2, 4 and 6 K, over the range 0–5 T. Dynamic susceptibility measurements were performed over the temperature range of 2–10 K, with a drive field of 3 Oe and a frequency range from 1 to 1488 Hz. Data were corrected for the diamagnetic contribution of the sample holder and eicosane by measurements and for the diamagnetism of the compounds.

Single Crystal X−ray Structural study

Single crystals of **1**, **2**, **4** and **5** were picked up with nylon loops and were mounted on a Bruker AXS D8 QUEST ECO diffractometer (at 296 K) equipped with a Mo−target rotating−anode X−ray source and a graphite monochromator (Mo−K_α, λ = 0.710 73 Å) while that of **3** was collected from a Bruker Nonius Apex II CCD diffractometer (at 296 K) with graphite monochromator and Mo−K_α radiation (λ = 0.71073 Å). Crystal structures were determined by direct methods and subsequent Fourier and difference Fourier syntheses, followed by full−matrix least squares refinements on F^2 using SHELXL −2017/1 software package.[23a] Crystal structure of **1** was refined with SHELXL −2017 within the Olex2−1.2 software package where one of the coordinated nitrate ion was modelled with PART instruction.[23b] The unit cell of **4** includes disordered solvent molecules which could not be modelled as discrete atomic sites therefore 'solvent mask' feature of Olex 2-1.2 was employed. PLATON/SQUEEZE was employed to calculate the diffraction contribution of solvent molecules which accounts possibly for the one water molecule per unit cell in non−stoichiometric occupancy (see ESI). Scaling and multiscan absorption corrections were employed using SADABS.[23c] Hydrogen atoms were located at their calculated position and refined isotropically, while the non hydrogen atoms were refined anisotropically. The hydrogen atom attached to oxygen was located in the difference Fourier map and refined isotropically. The crystallographic figures were generated using Diamond 3.0 software.[23d] The crystal parameters of the complexes are shown in Table S1 in the ESI. Metric parameters for complexes **1**−**5** are tabulated in Table S2−S6 in the ESI. CCDC: 1826188−1826190, 1826192 and 1826193 contain supplementary crystallographic data for this paper. These data can be obtained free of charge from the Cambridge Crystallographic Data Centre via www.ccdc.cam.ac.uk/data_request/cif.

Conflicts of interest

The authors have no relevant conflict of interest to declare.

Acknowledgements

YS and SG are thankful to Council of Scientific & Industrial Research (Sanction no. 09/028(0983)2016−EMR−I), India and Department of Science and Technology (DST−SERB) for the financial support respectively. DST−FIST and DST−PURSE is acknowledged for providing Single crystal XRD and ESI−MS facility at Department of Chemistry, University of Calcutta. We also like to thank CAS-V (UGC), Department of Chemistry, University of Calcutta for funding. We are also thankful to Prof. Prasanta Ghosh, Ramakrishna Mission Residential College (Autonomous), Narendrapur, India for providing the single crystal X−ray diffraction facility and Dr. Pinaki Saha for data collection. Department of Physics, University of Calcutta is acknowledged for providing the powder XRD measurement facilities. MM and MHO thank the University of Glasgow for financial support.

References

1 (a) R. Sessoli, D. Gatteschi, A. Caneschi and M. A. Novak, *Nature*, 1993, **365**, 141–143; (b) N. Ishikawa, M. Sugita , T. Ishikawa, S.−Y. Koshihara and Y. Kaizu, *J. Am. Chem. Soc.*, 2003, **125**, 8694–8695; (c) M. Hołyn´ska, D. Premuz˘ic´, I.−R. Jeon, W. Wernsdorfer, R. Clérac, and S. Dehnen, *Chem. Eur. J.*, 2011, **17**, 9605–9610.

2 (a) J. M. Frost, K. L. M. Harriman and M. Murugesu, *Chem. Sci.*, 2016, **7**, 2470–2491; (b) Y. Rechkemmer, F. D. Breitgoff, M. van der Meer, M. Atanasov, M. Hakl, M. Orlita, P. Neugebauer, F. Neese, B. Sarkar and J. V. Slageren, *Nat. Commun.*, 2016, **7**, 10467; (c) G. A. Craig and M. Murrie, *Chem. Soc. Rev.*, 2015, **44**, 2135– 2147.

3 Y.−Z. Zheng, G.−J. Zhou, Z. Zheng and R. E. P. Winpenny, *Chem. Soc. Rev.*, 2014, **43**, 1462−1475.

4 M. S. Fataftah, J. M. Zadrozny, S. C. Coste, M. J. Graham, D. M. Rogers and D. E. Freedman, *J. Am. Chem. Soc.*, 2016, **138**, 1344–1348.

5 M. Evangelisti, A. Candini, M. Affronte, E. Pasca, L. J. de Jongh, R. T. W. Scott, E. K. Brechin, *Phys. Rev. B*, 2009, **79**, 104414:1–104414:5.

6 (a) S. Brooker, *Chem. Soc. Rev.*, 2015, **44**, 2880–2892; (b) A. Bousseksou, G. Molnar, L. Salmon and W. Nicolazzi, *Chem. Soc. Rev.*, 2011, **40**, 3313–3335.

7 (a) M. H. Zeng, Z. Yi, Y. X. Tan, W. X. Zhang, Y. P. He, M. Kurmoo, *J. Am. Chem. Soc.*, 2014, **136**, 4680–4688; (b) R. Boča, J. Miklovič, J. Titiš, *Inorg. Chem.*, 2014, **53**, 2367–2369; (c) X. L. Wang, F. F. Sui, H. Y. Lin, J. W. Zhang, G. C. Liu, *Cryst. Growth Des.*, 2014, **14**, 3438–3452; (d) (f) S. Fortier, J. J. Le Roy, C. H. Chen, V. Vieru, M. Murugesu, L. F. Chibotaru, D. J. Mindiola, K. G. Caulton, *J. Am. Chem. Soc.*, 2013, **135**, 14670–14678; (e) D. Wu, D. Guo, Y. Song, W. Huang, C. Duan, Q. Meng and O. Sato, *Inorg. Chem.*, 2009, **48**, 854–860; (f) M. Murrie, *Chem. Soc. Rev.*, 2010, **39**, 1986–1995; (g) M. Kurmoo *Chem. Soc. Rev.*, 2009, **38**, 1353–1379; (h) D. Schweinfurth, M. G. Sommer, M. Atanasov, S. Demeshko, S. Hohloch, F. Meyer, F. Neese and B. Sarkar, *J. Am. Chem. Soc.*, 2015, **137**, 1993–2005.

View Article Online
DOI: 10.1039/C8NJ02955E

8 (a) R. Herchel, L. Vahovskaˊ, I. Potocňak, Z. Traˊvníček, *Inorg. Chem.*, 2014, **53**, 5896–5898; (b) Y.–Z. Zhang, A. J. Brown, Y.–S. Ming, H.–L Sun and S. Gao, *Dalton Trans.*, 2015, **44**, 2865–2870; (c) V. V. Novikov, A. A. Pavlov, Y. V. Nelyubina, M. Boulon, O. A. Varzatskii, Y. Z. Voloshin and R. E. P. Winpenny, *J. Am. Chem. Soc.*, 2015, **137**, 9792–9795; (d) R. Ruamps, L. J. Batchelor, R. Guillot, G. Zakhia, A.–L. Barra, W. Wernsdorfer, N. Guihery and T. Mallah, *Chem. Sci.*, 2014, **5**, 3418–3424.

9 (a) Y. –Y. Zhu, C. Cui, Y. –Q. Zhang, J. –H. Jia, X. Guo, C. Gao, K. Qian, S. –D. Jiang, B–W. Wang, Z. –M. Wang and S. Gao, *Chem. Sci.*, 2013, **4**, 1802–1806; (b) C. Zhang, Z. –Y. Liu, N. Liu, N. Liu, H. Zhao, E. –C. Yang and X. –J. Zhao, *Dalton Trans.*, 2016, **45**, 11864–11875; (c) M. R. Saber and K. R. Dunbar, *Chem. Commun.*, 2014, **50**, 12266–12669; (d) Y. –Z. Zhang, S. Gómez–Coca, A. J. Brown, M. R. Saber, X. Zhang and K. R. Dunbar, *Chem. Sci.*, 2016, **7**, 6519–6527; (e) R. Boča, J. Miklovič and J. Titiš, *Inorg. Chem.*, 2014, **53**, 2367–2369; (f) Y. Y. Zhu, C. Cui, Y.–Q. Zhang, J.–H. Jia, X. Guo, C. Gao, K. Qian, S.–D. Jiang, B.–W. Wang, Z.–M. Wang and S. Gao, *Chem. Sci.*, 2013, **4**, 1802–1806; (g) J. M. Zadrozny, J. Telser and J. R. Long, *Polyhedron*, 2013, **64**, 209–217; (h) F. Yang, Q. Zhou, Y. Zhang, G. Zeng, G. Li, Z. Shi, B. Wang and S. Feng, *Chem. Commun.*, 2013, **49**, 5289–5291; (i) R. Ruamps, L. J. Batchelor, R. Maurice, N. Gogoi, P. Jimenez–Lozano, N. Guihery, C. de Graaf, A. L. Barra, J. P. Sutter and T. Mallah, *Chem. Eur. J.*, 2013, **19**, 950–956; (j) M. Idešicová, J. Titiš, J. Krzystek and R. Boča, *Inorg. Chem.*, 2013, **52**, 9409–9417; (k) W. Huang, T. Liu, D. Wu, J. Cheng, Z. W. Ouyang and C. Duan, *Dalton Trans.*, 2013, **42**, 15326–15331; (l) F. Habib, O. R. Luca, V. Vieru, M. Shiddiq, I. Korobkov, S. I. Gorelsky, M. K. Takase, L. F. Chibotaru, S. Hill, R. H. Crabtree and M. Murugesu, *Angew. Chem., Int. Ed.*, 2013, **52**, 11290–11293; (m) J. M. Zadrozny, J. J. Liu, N. A. Piro,C. J. Chang, S. Hill and J. R. Long, *Chem. Commun.*, 2012, **48**, 3927–3929; (n) J. Vallejo, I. Castro, R. Ruiz–García, J. Cano, M. Julve, F. Lloret, G. De Munno, W. Wernsdorfer and E. Pardo, *J. Am. Chem. Soc.*, 2012, **134**, 15704–15707; (o) S. A. Cantalupo, S. R. Fiedler, M. P. Shores, A. L. Rheingold and L. H. Doerrer, *Angew. Chem., Int. Ed.*, 2012, **51**, 1000–1005; (p) J. M. Zadrozny and J. R. Long, *J. Am. Chem. Soc.*, 2011, **133**, 20732–20734; (q) D. Weismann, Y. Sun,Y. Lan, G. Wolmershäuser, A. K. Powell and H. Sitzmann, *Chem. Eur. J.*, 2011, **17**, 4700–4704; (r) T. Jurca, A. Farghal, P. H. Lin, I. Korobkov, M. Murugesu and D. S. Richeson, *J. Am. Chem. Soc.*, 2011, **133**, 15814–15817; (s) E.–C. Yang, D. N. Hendrickson, W. Wernsdorfer, M. Nakano, L. N. Zakharov, R. D. Sommer, A. L. Rheingold, M. Ledezma–Gairaud and G. Christou, *J. Appl. Phys.*, 2002, **91**, 7382–7384; (t) K. W. Galloway, A. M. Whyte, W. Wernsdorfer, J. Sanchez–Benitez, K. V. Kamenev, A. Parkin, R. D. Peacock and M. Murrie, *Inorg. Chem.*, 2008, **47**, 7438–7442; (u) Y. Z. Zhang, W. Wernsdorfer, F. Pan, Z. –M. Wang and S. Gao, *Chem. Commun.*, 2006, 3302–3304; (v) A. Ferguson, A. Parkin, J. Sanchez–Benitez, K. Kamenev, W. Wernsdorfer and M. Murrie, *Chem. Commun.*, 2007, **0**, 3473–3475; (w) Y.–Z. Zheng, M. Speldrich, H. Schilder, X.–M. Chen and P. Kogerler, *Dalton Trans.*, 2010, **39**, 10827–10829.

10 G. Aromíˊ, S. Bhaduri, P. Artuˊs, K. Folting and G. Christou, *Inorg. Chem.*, 2002, **41**, 805–817.

11 (a) S. –N. Zhao, S. –Q. Su, X. –Z. Song, M. Zhu, Z. –M. Hao, X. Meng, S. –Y. Song and H. –J. Zhang, *Cryst. Growth Des.*, 2013, **13**, 2756–2765; (b) P. Lama, J. Mrozinski and P. K. Bharadwaj, *Cryst. Growth Des.*, 2012, **12**, 3158–3168; (c) H. Wang, D. Zhang, D. Sun, Y. Chen, L. –F. Zhang, L. Tian, J. Jiang, Z. –H. Ni, *Cryst. Growth Des.*, 2009, **9**, 5273–5282.

12 a) S. G. Sreerama and S. Pal, *Inorg. Chem.*, 2005, **44**, 6299–6307; (b) L. Yan , S. Ding , Y. Ji , Z. Liu and C. Liu, *J. Coord. Chem.*, 2011, **64**, 3531–3540; (c) M. Hong, F. Chen–jie, D. Chun–ying, L. Yu–ting and M. Qing–jin, *Dalton Trans.*, 2003, **0**, 1229 – 1234.

13 (a) M. Andruh, *Dalton Trans.*, 2015, **44**, 16633–16653; (b) M. Heras Ojea, M. A. Hay, G. Cioncoloni, G. A. Craig, C. Wilson, T. Shiga, H. Oshio, M. D. Symes and M. Murrie, *Dalton Trans.*, 2017, **46**, 11201–11207.

14 (a) R. Modak, Y. Sikdar, G. Cosquer, S. Chatterjee, M. Yamashita and S. Goswami, *Inorg. Chem.*, 2016, **55**, 691–699; (b) R. Modak, Y. Sikdar, A. E. Thuijs, G. Christou and S. Goswami *Inorg. Chem.*, 2016, **55**, 10192–10202.

15 (a) P. –H. Lin, T. J. Burchell, L. Ungur, L. F. Chibotaru, W. Wernsdorfer and M. Murugesu, *Angew. Chem. Int. Ed.* 2009, **48**, 9489 –9492; (b) L.–F. Zou, L. Zhao,Y.–N. Guo, G.–M. Yu, Y. Guo, J. Tang and Y.–H. Li, *Chem. Commun.*, 2011, **47**, 8659–8661; (c) J. Wu, L. Zhao, P. Zhang, L. Zhang, M. Guo and J. Tang, *Dalton Trans.*, 2015, **44**, 11935–11942; (d) M.–L. Wei, J.–J. Sun, and X.–Y. Duan, *Eur. J. Inorg. Chem.*, 2014, 345–351. (e) W. –Q. Lin, J. –D. Leng and M. –L. Tong, *Chem. Commun.*, 2012, **48**, 4477–4479.

16 (a) S. K. Langley, B. Moubaraki, C. Tomasi, M. Evangelisti, E. K. Brechin and K. S. Murray, *Inorg. Chem.*, 2014, **53**, 13154–13161, (b) M. Pait, A. Bauzá, A. Frontera, E. Colacio, and D. Ray, *Inorg. Chem.*, 2015, **54**, 4709–4723.

17 C.–D. Si, D.–C. Hu, Y. Fan, X.–Y. Dong, X.–Q. Yao, Y.–X. Yang, and J.–C. Liu *Cryst. Growth Des.*, 2015, **15**, 5781–5793.

18 A. K. Sharma, F. Lloret, and R. Mukherjee, *Inorg. Chem.*, 2013, **52**, 4825–4833.

19 M. Pinsky and D. Avnir, *Inorg. Chem.*, 1998, **37**, 5575–5582.

20 D. Casanova, M. Llunell, P. Alemany and S. Alvarez, *Chem. Eur. J.*, 2005, **11**, 1479–1494.

21 S. Alvarez and M. Llunell, *J. Chem. Soc.*, *Dalton Trans.*, 2000, 3288–3303.

22 G. Aromi, A. Batsanov, P. Christian, M. Helliwell, A. Parkin, A. A. Smith, G. A. Timco and R. E. P. Winpenny, *Chem. Eur. J.*, 2003, **9**, 5142–5161.

23 (a) G. M. Sheldrick, *Acta Cryst.* A64, 112-122, (b) O. V. Dolomanov, L. J. Bourhis, R. J Gildea, J. A. K. Howard and H. Puschmann, A complete structure solution, refinement and analysis program, *J. Appl. Cryst*, 2009, **42**, 339-341. (c) G. M. Sheldrick, SADABS, a software for empirical absorption correction, Ver. 2.05; University of Göttingen: Göttingen, Germany, 2002; (d) K. Bradenburg, Diamond, ver. 3.0; Crystal Impact GbR: Bonn, Germany, 2005.

View Article Online
DOI: 10.1039/C8NJ02955E

Graphical abstract

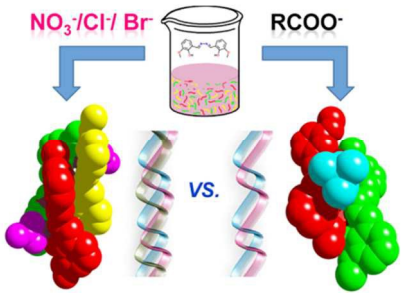

Triple helical Co^{II}_4 and double helical Co^{II}_3 from diazine based ligand synthesized and their magnetic behavior rationalized by susceptibility measurement.